LEVEL II

SGI-R-79-002

SEISMIC SOURCE FUNCTIONS AND ATTENUATION FROM LOCAL AND TELESEISMIC OBSERVATIONS OF THE NTS EVENTS JORUM AND HANDLEY

D. M. HADLEY

QUARTERLY TECHNICAL REPORT

FOR PERIOD NOVEMBER 22, 1978 - JANUARY 31, 1979

SPONSORED BY

DEFENSE ADVANCED RESEARCH PROJECTS AGENCY (DOD)

ARPA ORDER No. 2551

This research was supported by the Advanced Research Projects Agency of the Department of Defense and was monitored by AFTAC/VSC, Patrick AFB, FL. 32925, under Contract No. F08606-79-C-0009.

March 8, 1979

SIERRA GEOPHYSICS, INC.

150 N. SANTA ANITA AVENUE • ARCADIA, CALIFORNIA 91006 • (213) 574-7052

AFTAC Project Authorization: VT/9710

ARPA Order: 2551

Effective Date of Contract: November 22, 1978

Contract Expiration Date: September 30, 1979

Contract No: F08606-79-0009

Principal Investigators and Phone No:

Dr. Robert S. Hart

Dr. David M. Hadley

Dr. Rhett Butler

(213) 574-7052

Program Manager and Phone No:

Mr. Michael J. Shore

(202) 325-7581

Unclassified

SECURITY CLASSIFICATION OF THIS PAGE (When Data Entered)

REPORT DOCUMENTATION PAGE		READ INSTRUCTIONS BEFORE COMPLETING FORM
1. REPORT NUMBER	2. GOVT ACCESSION NO.	3. RECIPIENT'S CATALOG NUMBER
4. TITLE (and Subtitle) Seismic Source Functions and Attenuation from Local and Teleseismic Observations of the NTS Events Jorum and Handley		5. TYPE OF REPORT & PERIOD COVERED Quarterly Technical Rpt. 11/22/78 - 1/31/79
		6. PERFORMING ORG. REPORT NUMBER SGI-R-79-002
7. AUTHOR(s) David M. Hadley		8. CONTRACT OR GRANT NUMBER(s) Contract Number F08606-79-0009
9. PERFORMING ORGANIZATION NAME AND ADDRESS Sierra Geophysics, Inc. 150 No. Santa Anita Ave. Arcadia, CA 91006		10. PROGRAM ELEMENT, PROJECT, TASK AREA & WORK UNIT NUMBERS ARPA Order No. 2551
11. CONTROLLING OFFICE NAME AND ADDRESS VELA Seismological Center 312 Montgomery Street Alexandria, VA 22314		12. REPORT DATE March 8, 1979
		13. NUMBER OF PAGES 35
14. MONITORING AGENCY NAME & ADDRESS(if different from Controlling Office)		15. SECURITY CLASS. (of this report) Unclassified
		15a. DECLASSIFICATION/DOWNGRADING SCHEDULE

16. DISTRIBUTION STATEMENT (of this Report)

Approved for public release, distribution unlimited

17. DISTRIBUTION STATEMENT (of the abstract entered in Block 20, if different from Report)

18. SUPPLEMENTARY NOTES

19. KEY WORDS (Continue on reverse side if necessary and identify by block number)

Underground Nuclear Explosions
Seismic Source Functions
Attenuation
Body Waves

20. ABSTRACT (Continue on reverse side if necessary and identify by block number)

This technical report discusses the determination of an accurate source description for Jorum and the results are extended to the teleseismic observations of Handley. The basic data set used to model the source are the strong motion accelerograms collected by Peppin (1964) at a distance of 8 kilometers from the test. At this distance the initial seismic energy represents diving rays and the observations are suitable for comparison with more distant regional and teleseismic observations. Using a

DD FORM 1 JAN 73 1473 EDITION OF 1 NOV 65 IS OBSOLETE

Unclassified 61393 821

SECURITY CLASSIFICATION OF THIS PAGE (When Data Entered)

modified Von Seggern and Blandford (1972) source representation, and including near-field terms, it has been possible to obtain a source function which not only accurately models the close-in records but also matches teleseismic observations. After defining the near-field explosion source description, a t* for teleseismic observations is calculated. For WWSSN short and long period observations of these events, we obtain an average t* of about 1.3 for compressional waves with a scatter of about ±0.2. There are systematic azimuthal trends in the observed t* values which are not strongly correlated with the Silent Canyon caldera but may be correlated with upper mantle structure northeast of NTS. These data do not rule out systematic receiver function bias as the cause of the amplitude variations.

plus or minus

(14) SGI-R-79-002

(6) SEISMIC SOURCE FUNCTIONS AND ATTENUATION FROM LOCAL AND TELESEISMIC OBSERVATIONS OF THE NTS EVENTS JORUM AND HANDLEY.

(10) David [redacted] M./ HADLEY

(9) QUARTERLY TECHNICAL REPORT, 22 NOV 78 - 31 Jan 79

FOR PERIOD NOVEMBER 22, 1978 - JANUARY 31, 1979

SPONSORED BY

DEFENSE ADVANCED RESEARCH PROJECTS AGENCY (DOD)

ARPA ORDER NO. 2551

This research was supported by the Advanced Research Projects Agency of the Department of Defense and was monitored by AFTAC/VSC, Patrick AFB, FL. 32925, under Contract No. F08606-79-C-0009, (15) ARPA Order-2551

(11) 8 Mar [redacted] 79 (12) 42 p.

393 821

TABLE OF CONTENTS

List of Illustrations

TECHNICAL SUMMARY

An important initial task in the time domain analysis of observed yield bias at NTS is the determination of a reliable seismic source function of underground nuclear explosions. This function needs to be appropriate for local, regional, and teleseismic observational distances. Given such a source description we may then proceed to separate the effects of anelastic dissipation, commonly characterized by the parameter t* (the ratio of observed travel-time to apparent attenuation), receiver structure, and crustal structure in the near-source environment. Without an adequate source parameterization, the source characteristics and those propagational factors will be hopelessly intertwined.

This technical report discusses the determination of an accurate source description for Jorum and the results are extended to the teleseismic observations of Handley. This source function has then been used to estimate local crustal structure and indicate important areas of further study and geophysical exploration, and, finally to help examine amplitude and apparent yield variations in the Pahute Mesa area of the Nevada Test Site.

The basic data set used to model the source were the strong motion seismograms collected by Peppin (1964). These seismograms were recorded at about 8 kilometers from the test sites. This distance is far enough removed that the influence of highly non-

linear near-field effects such as spall and minor movement along fractures do not dominate the record but yet close enough that clear signals were recorded. Moreover, at this distance the initial seismic energy represents diving rays and hence is suitable for comparison with more distant regional and teleseismic observations. Using a modified Von Seggern and Blandford (1972) source representation, and including near-field terms, it has been possible to obtain source functions which not only accurately model close-in records but also match teleseismic observations. Having once defined the explosion source description, it is a straightforward task to determine the effective t* for teleseismic observations without the usual ambiguity of what are the source influences as opposed to the anelastic effects. For WWSSN short period observations of these events, we obtain an average t* of about 1.3 for compressional waves with a scatter of about ±0.2. There are systematic azimuthal trends in the observed t* values which are not strongly correlated with the Silent Canyon caldera but may be correlated with part of the central Rocky Mountains. It is not possible at this time to rule out systematic receiver function biases as the cause of the amplitude variations. A principal, although for present purposes not critical, limitation on the source function determination made in this study is the uncertainties in the precise crustal structure and seismological properties along the 8 km paths between the events and the strong motion sites. Since these uncertainties directly affect the

resolved source function (as described in detail within this report), this structure needs to be more precisely defined in our efforts to reduce the observed yield variations at NTS.

INTRODUCTION

In recent years, there have been a number of attempts at comparing local strong motion data with teleseismic observations. In the case of explosions, investigators have examined the frequency content of short period P waves to measure attenuation (for example, Fraiser and Filson, 1972). They estimate t* to be about (.5) where $t^*_\alpha = \frac{T}{Q\alpha}$ = (Travel time of compressional (α) wave /$Q\alpha$). If t* is known along some ray path, then a convolution operator A(r,t*) can be constructed to correct a seismic pulse for attenuation [Carpenter et al. (1967)].

In the case of earthquake data, occasionally both long and short period P and S waves at teleseismic distances and well-recorded local S waves are available. The long period pulses are easily modeled synthetically, see, for example, Burdick and Mellman (1976). Their results for the Borrego Mountain earthquake indicate that the direct P wave actually contains P, pP and sP, with the latter phase dominating. Modeling the phases sP and sS, Burdick (1978) estimated t^*_β to be 5.2. Heaton and Helmberger (1977) modeled the strong motion data and found that Burdick's teleseismic description of Borrego was compatible with the local observations.

In general, comparing seismic pulses at various locations produced by earthquakes with the intent of determining Q is particularly difficult because of source finiteness and associated directivity effects. The complex radiation pattern associated with earthquakes introduces large uncertainties in comparing waveforms from various stations. With the goal of

avoiding this problem, we have reworked some of the best data available by comparing observations made near large nuclear explosions with teleseismic measurements of short and long period P waves.

NEAR FIELD STUDIES

The megaton events considered in this study were located on the Pahute Mesa of the Nevada Test Site, (NTS), see Figure 1. The near field data described by Peppin (1974), was recorded at several azimuths at a distance of 8 km. The local data represent a reversed profile with Jorum shooting west and Handley towards the east. Complete recordings made at this distance are generally easier to obtain since the violent motions associated with some very near field phenomena are absent. The results for the Jorum experiment are given in Figure 2; however, the reverse Handley experiment was not as successful. The records are similar to those in Figure 2, but are slightly clipped on the first down swing, see Peppin (1974).

The energy in the first arrivals at stations 4, 5, and 6, Figure 2, is concentrated on the vertical component, but, as time progresses, shifts to the radial. Also, note that many of the later arrivals are not particularly coherent from site to site, as can be seen by comparing any individual trace with the average stack shown on the bottom of Figure 2. These observed features can be explained by an initial downgoing P wave, with an incidence angle at the stations of about 30° yielding a radial to vertical ratio of about .4. The later arrivals travel in the slower surface layers. These later arrivals probably contain abundant information about the source-surface interaction, slapdown, tectonic release, slippage along cracks, and other complex phenomena. We will concentrate

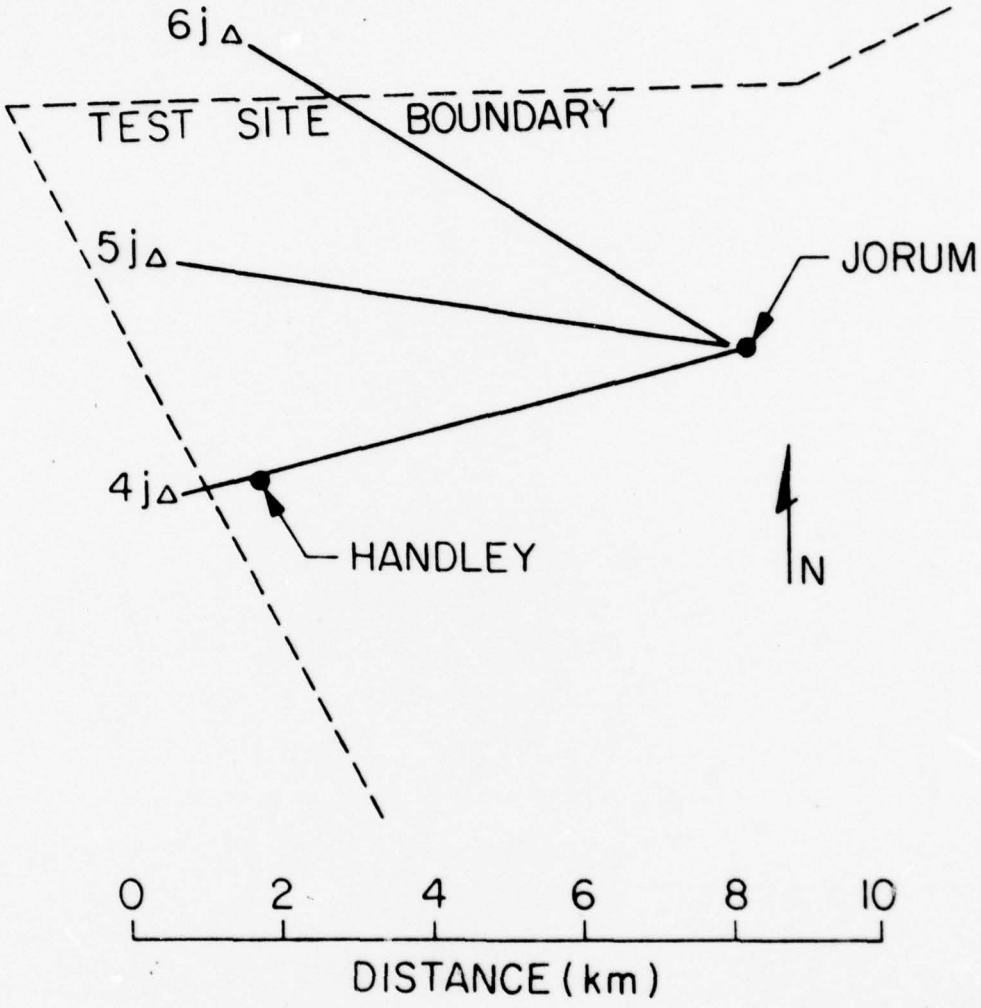

Figure 1: Map of NTS showing accelerometer locations for the Jorum and Handley tests, modified from Peppin (1974).

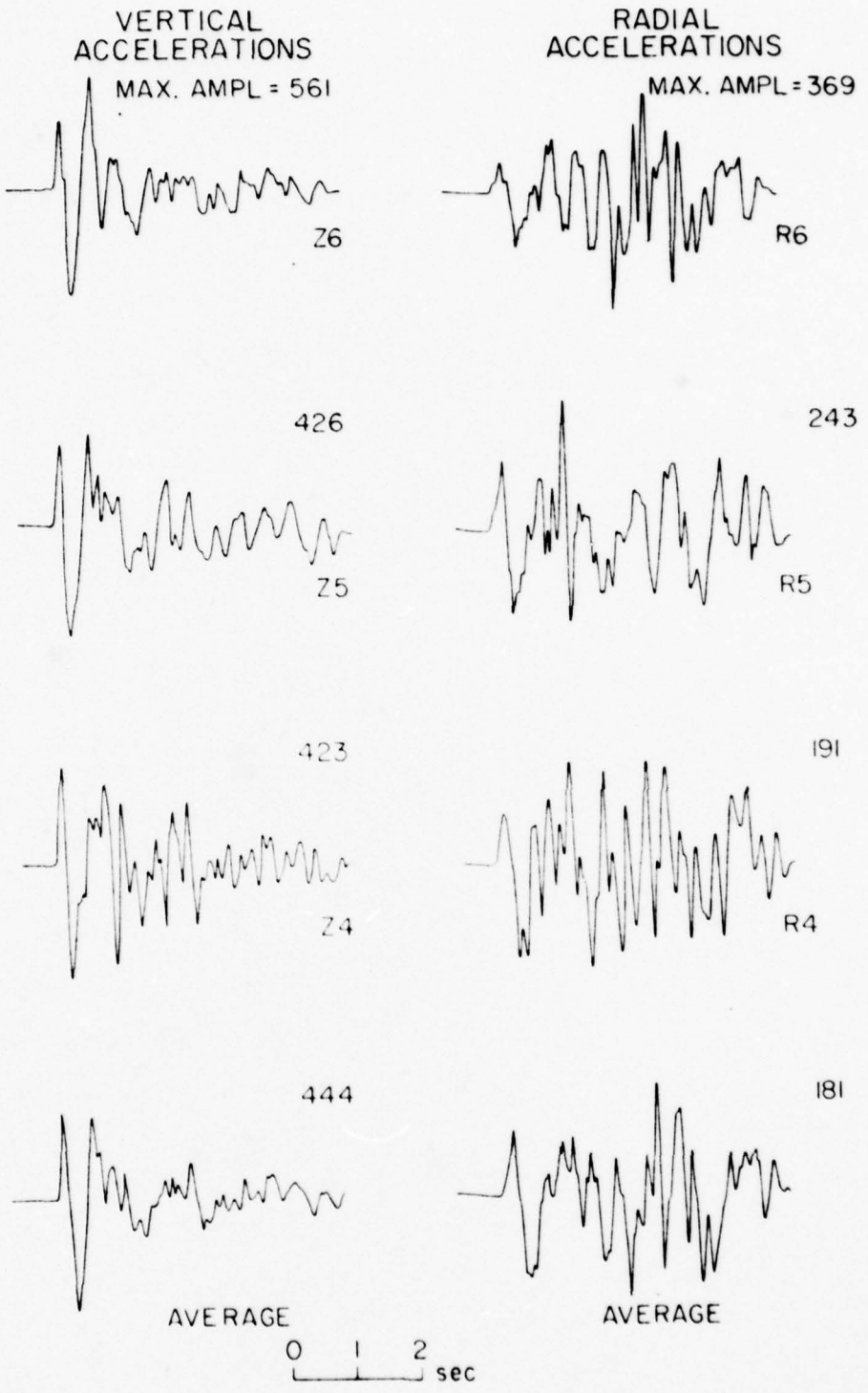

Figure 2: Vertical and radial accelerograms at sites 6, 5, and 4 with peak amplitudes given above each trace. The bottom traces are the stacked averages of the vertical and radial components, respectively.

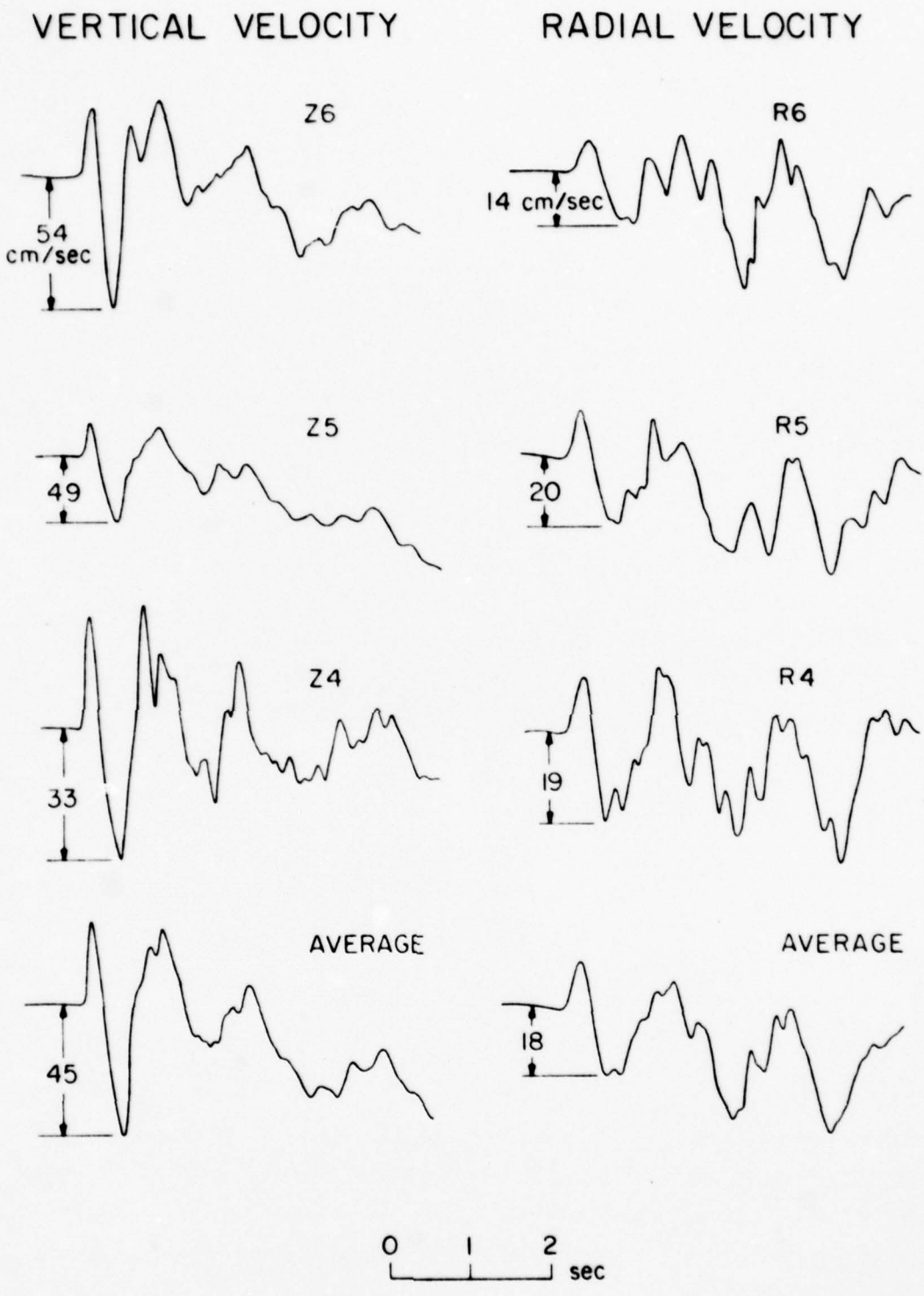

Figure 3: Vertical and radial velocities obtained by integrating the accelerograms displayed in Figure 2.

our efforts in this paper on the first-cycle of motion which we interpret as representative of the dominant out-going signals. For modeling purposes, it is convenient to work with the integral of these acceleration measurements as displayed in Figure 3. We have not removed the linear drift that occurs in this operation because we will only work with the first cycle. Furthermore, the instruments are sufficiently broad-band that the initial velocity pulse can be treated as the true ground motion [McEvilly (personal communication)]. Thus, the first second of the average vertical velocity component along with the corresponding teleseismic observations, Figure 4, will be our prime data set for determining t*.

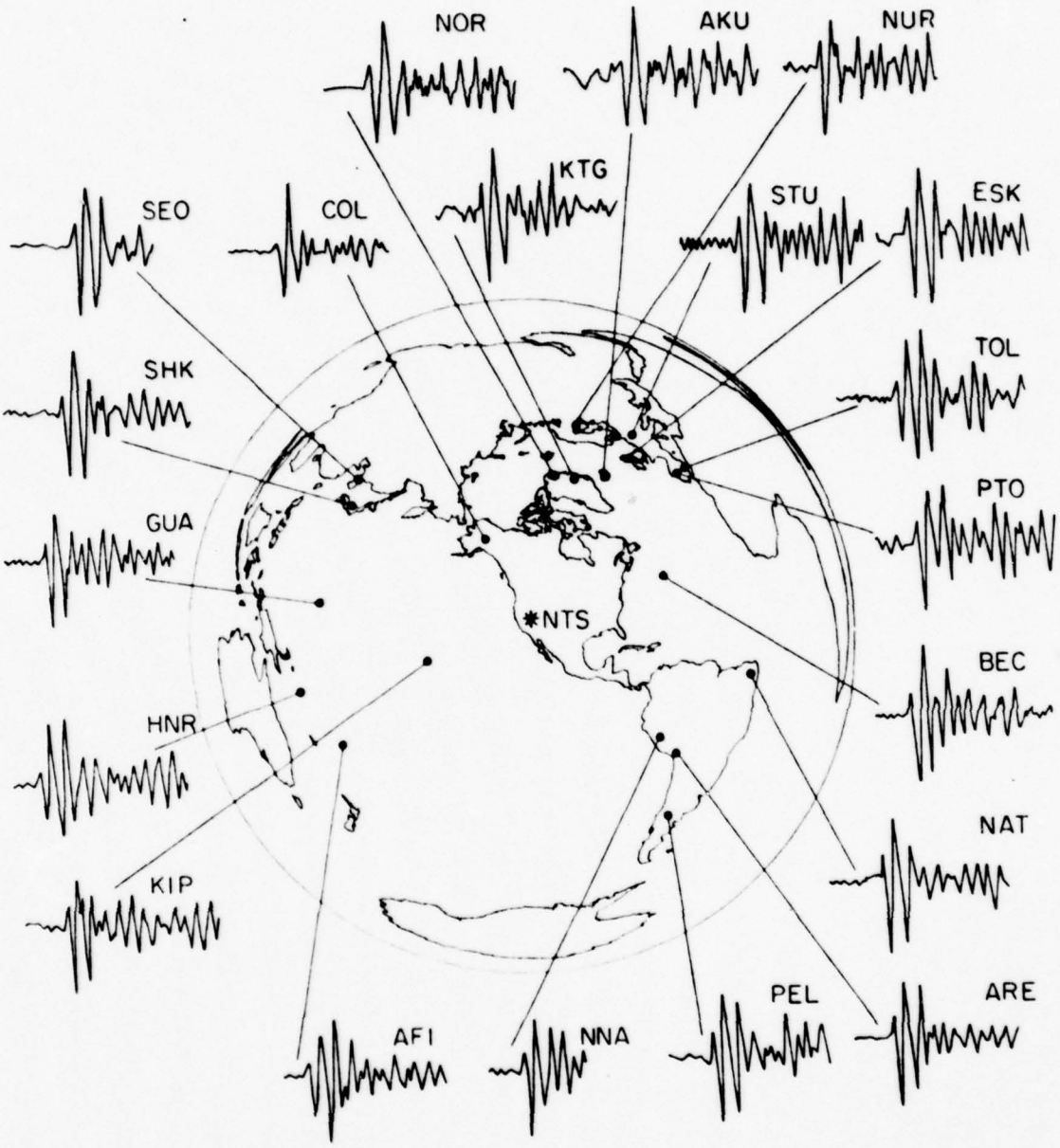

Figure 4: Station location and P-waves obtained from the WWSSN Network. Absolute amplitude data are listed in Table 1.

NEAR FIELD MODELING TECHNIQUES

The techniques for modeling teleseismic explosion waveforms have been discussed at length by numerous authors with one of the latest expositions given by Burdick and Helmberger (1979). Assuming an elastic layered earth with $t^* = 1$, they find that large overshoots of at least 2 to 1 in the reduced displacement potential, RDP, will explain most of the short and long period observations of both the Soviet and U.S. explosions. The Burdick and Helmberger study used the RDP proposed by Von Seggern and Blandford (1972) expressed by

$$\psi(t) = \psi(\infty)\left[1 - e^{-Kt}(1 + Kt - B(Kt)^2)\right] \qquad (1)$$

where $\psi(\infty)$ is the source strength, K scales inversely as cube root of the yield, and B is the overshoot constant. With $B > 2$ the data is well modeled without adding a slapdown phase or related phenomena. It should be noted that, since we are treating the phase pP as an elastic interaction, the combined radiation of P plus pP is a simple parameterization and that any combination of RDP's with a non-elastic reflection of pP which yields an equivalent overshoot behavior will be acceptable in fitting the teleseismic data.

The displacement potential is given by

$$\phi(R,t) = -\psi(t)/R \qquad (2)$$

and the displacement by

$$D(R,t) = \psi(t)/R^2 + (1/R\alpha)(d\psi(t)/dt), \qquad (3)$$

where R is the radial distance and α is the velocity. In terms of generalized ray theory, the vertical displacement for a layered earth becomes

$$D(r,z,t) = - (d\psi/dt * dS/dt) \qquad (4)$$

where the step response of the model is given by

$$S(t) = \frac{2}{r}\frac{1}{\pi}\left[\frac{1}{\sqrt{t}} * \Sigma \text{ rays}\right] \qquad (5)$$

see Helmberger and Harkrider (1972). The velocity component can be written as

$$V(t) = - \frac{d}{dt} (d\psi/dt * dS/dt) \qquad (6)$$

$$= - (d^2\psi/dt^2 * dS/dt) \qquad (7)$$

$$= - (d^3\psi/dt^3 * S) \qquad (8)$$

$$= - \frac{d}{dt} (d^2\psi/dt^2 * S) \qquad (9)$$

Mathematically (6) through (9) are equivalent, but numerically

and geophysically the order of operations can effect the results. At teleseismic distances, the delta response of the earth, dS/dt, is reasonably well known and thus, expression (6) is commonly used. For this reason, one does not worry about the fact that $(d^2\psi/dt^2)$ of the expression (1) is ill-behaved. In our present situation, we do not know the local structure at Jorum particularly well and, consequently, our knowledge of S(t) at the short periods is lacking and the operation (dS/dt) should be avoided. We can accomplish this by demanding more of $\psi(t)$ or by adding another term in the original Haskell (1967) description, namely,

$$\psi(t) = \psi_o \left[1 - e^{-Kt}(1 + (Kt) + 1/2(Kt)^2 - B(Kt)^3)\right] \qquad (10)$$

and applying (9) in modeling the velocity pulse displayed in Figure 3. To compute S(t) we need to have an accurate layered model of the source region, which we consider next.

LOCAL CRUSTAL MODEL

A detailed velocity model of the Silent Canyon Caldera and Pahute Mesa would be rather complex. With increasing depth, the lithologic units grade from bedded and ash flow tuffs to interbedded tuffs and lava flows to lavas and intrusives with intermediate composition [Orkild and others (1969)]. We have attempted to represent this complex with a four layer model, Figure 5. The surficial layer is an average velocity from an acoustic log obtained in a shallow borehole in the Oak-Spring tuff at the NTS [Keller (1960)]. The depth to the bottom of this unit coincides with the position of the static water table [Springer and Kinnaman (1971)]. The velocities of the next two units (3.4 and 3.8 km/sec) are consistent with both a decrease in the tuff content with increasing depth and the report by Spence (1974) of an average caldera velocity of 3.6 km/sec. Finally, the velocity of the half space is intermediate between the velocity of the pre-Cenozoic rocks that surround Pahute Mesa and the lavas and intrusions comprising the lower sections of the caldera [Spence (1974), Diment and other (1960)]. Depth to the top of this layer is approximately located from geologic sections constructed from borehole data [Orkild and others (1969)].

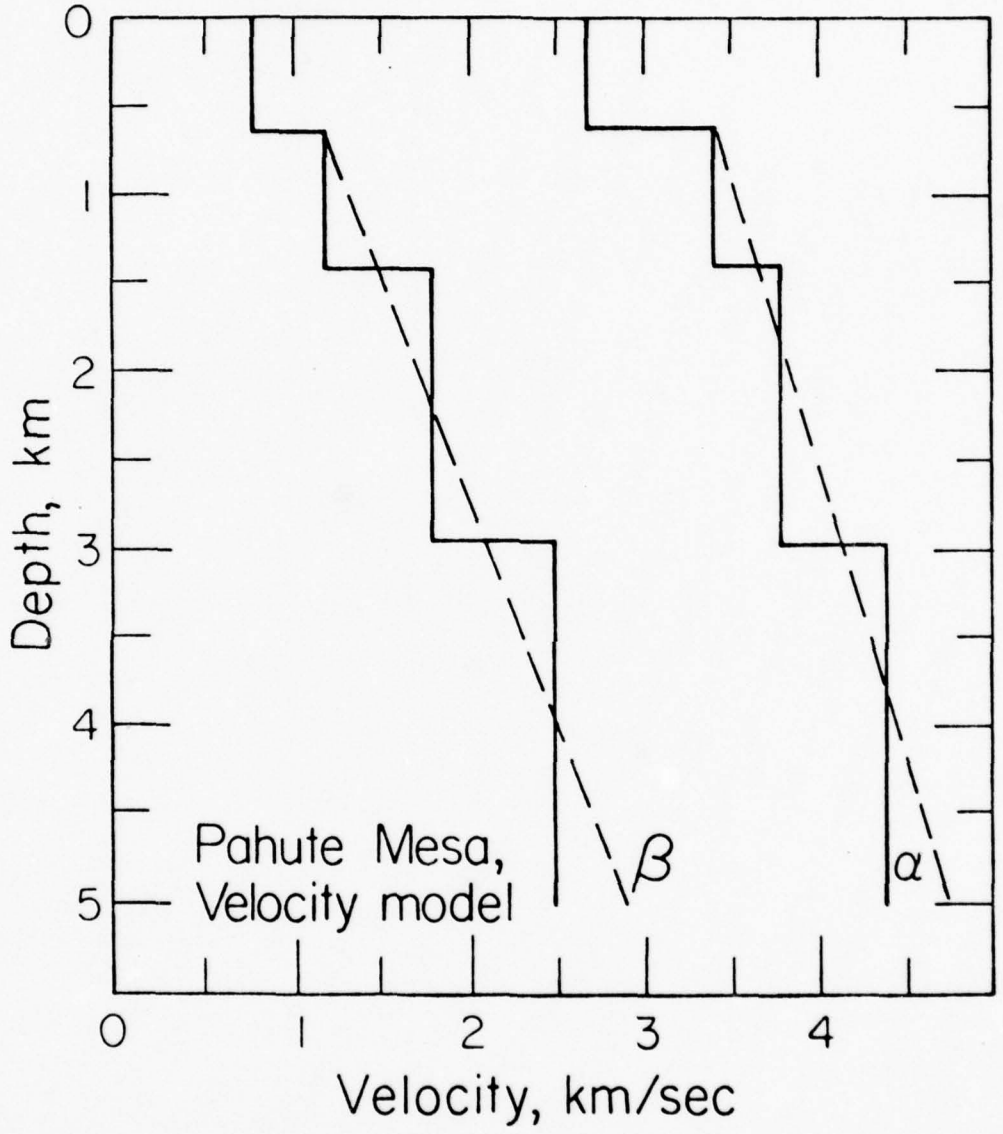

Figure 5: Crustal models constructed for the Pahute Mesa test site. The hard top model referred to in the text assumes that $\beta_1 = \beta_2 = 1.2$ km/sec., i.e. no change in shear velocity above a depth of 1.5 km.

MODELING THE STRONG MOTION RECORDS

Synthetic velocity waveforms based on the above model for a range of distances are presented in Figure 6. A slightly smoothed (dS/dt) is included to display the roughness of the response caused by the layering. Note that the phase pP, which becomes a strong feature beyond about 5 km, interacts with the overshoot feature of the source. In these synthetics we have included only generalized rays that arrive within the first second of motion. In Figure 7 we compare various assumed K and B values with the observed vertical waveshape in overlay form. Most of these fits could be considered adequate except, perhaps, for (B = 2, K = 4), which is somewhat too broad. It should be noted that the ratio of radial to vertical motions shown in Figure 6 is about .45, whereas the average for the data is somewhat lower, with considerable variation for the individual recordings, see Figure 3. Also, note that when the downswing is particularly large, station 6 on Figure 3, we obtain a relatively low ratio of radial to vertical motion. Thus, to gain some insight, we ran several additional models with the results displayed in the left two columns of Figure 8. Since the radial shapes were quite similar to the verticals, we have plotted only the vertical component and the amplitude ratio. First, we note that increasing the shear velocity in the surface layer (hard top) greatly affects the ratio as well as changes the strength of pP. When the surface is soft (low shear velocity) we obtain a strong pP

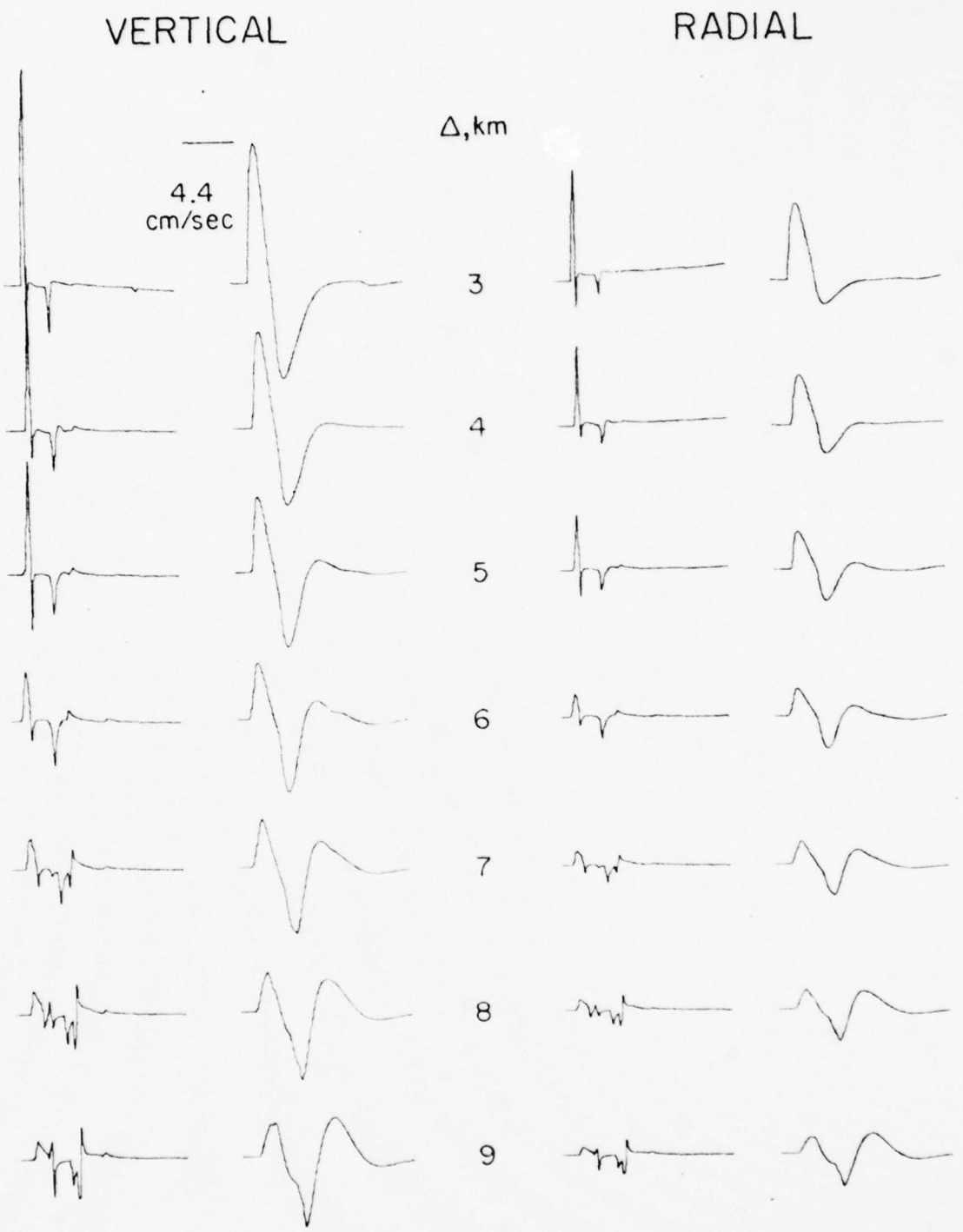

Figure 6: Vertical and radial Green's functions and velocity responses assuming (K = 5, B = 2) for the layered model given in Figure 5.

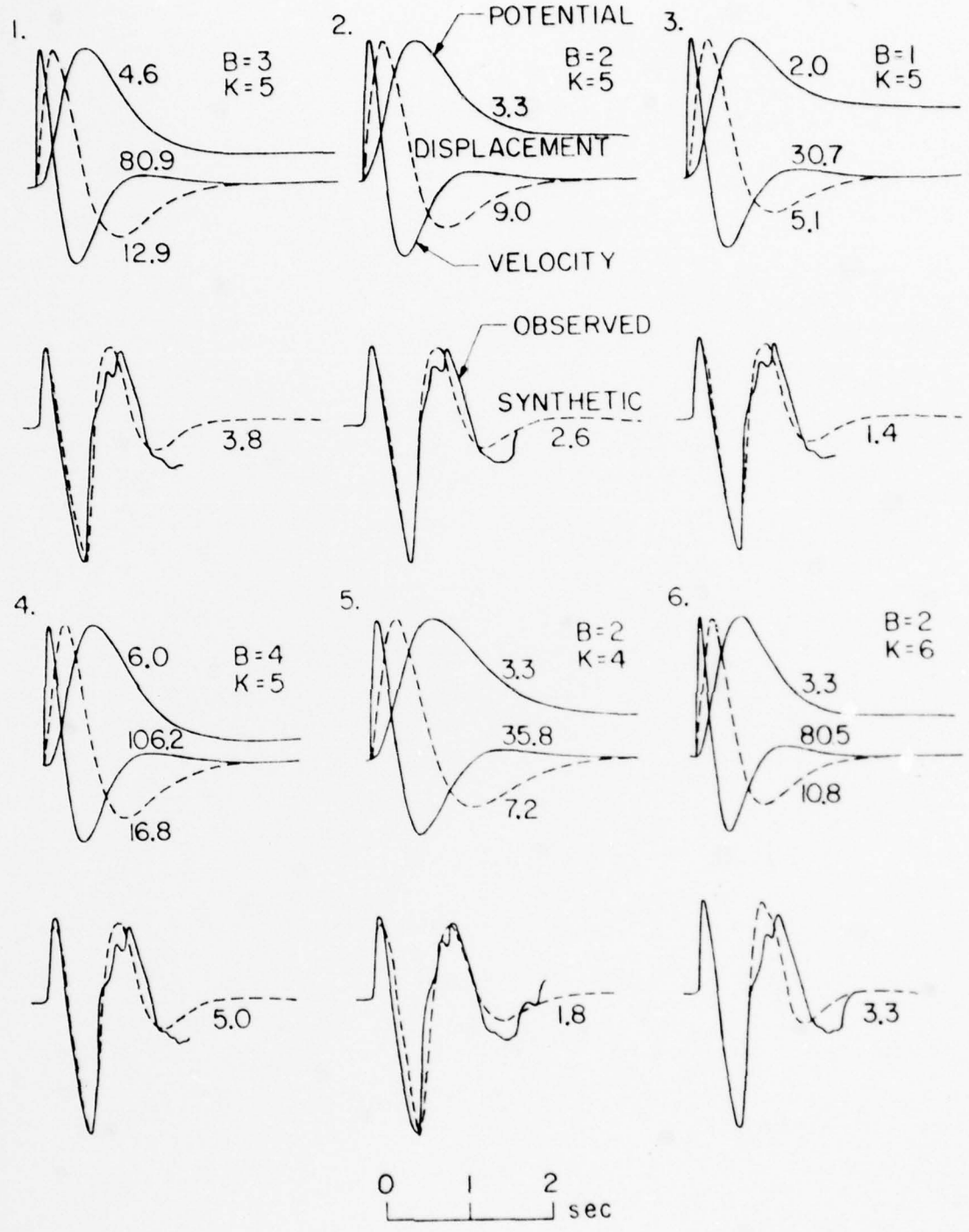

Figure 7: A comparison of synthetic velocity responses with the average vertical observation (shown in Figure 3) for various values of the K and B parameters.

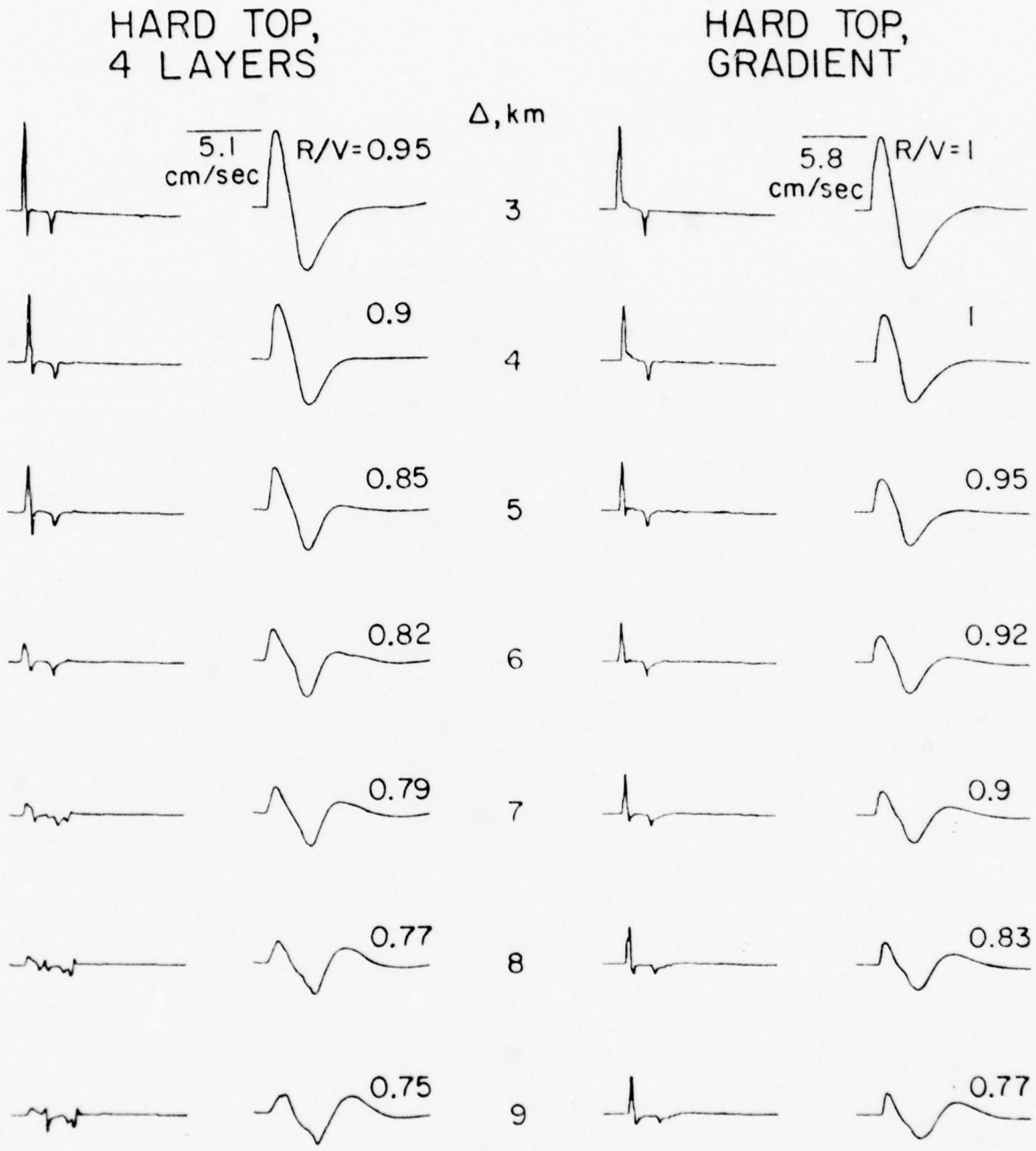

Figure 8: Green's functions and synthetic velocity responses for (K = 5, B = 2), assuming the layered model and smooth gradient model with the hard top.

because of the weak conversion to pS and, secondly, a soft surface has a strong effect on the receiver function. Thus, a strong pP is compatible with a small ratio of radial to vertical and it appears that Figure 3 can be interpreted in this fashion. Another interesting feature that is common to the waveshapes in Figure 3 is a relatively broader upswing on the radial relative to vertical components. This feature is not particularly important to our objective, but we have produced models that give this effect by including a thin soft layer at the surface and including rays that convert from P to SV near the receiver. The radial component is strongly affected by these types of conversions, whereas the vertical component is rather insensitive.

To test the sensitivity of our synthetics to the choice of model parameters, Green's functions for a second velocity model were also computed. The new model replaces the lower three layers with a linear gradient, Figure 5. The computed Green's functions are shown in the right side of Figure 8. Although the shapes of the new response functions are slightly different, the convolution with the longer period source function produces waveforms and amplitude ratios that are very comparable with the discrete model.

A problem that might affect our results would be the presence of thin high velocity layers above the source. Such a structure could produce tunnelling effects and strongly reduce the shorter period amplitudes. Fortunately, at $\Delta = 8$ km

the turning velocity approaches 3.8 km/sec and this velocity should be sufficiently high to avoid that problem (see Mellman and Helmberger, 1974). If significant high velocity layers are actually present above the source, then the source strength would be underestimated and the teleseismic t* would be slightly overestimated.

In conclusion, the crustal model below the shot point down to about 4 km controls the amplitude of the synthetics. The delay time of pP is consistent with the model given in Figure 5. A smooth gradient model gives about the same results. Thus, we can determine $\psi_o(K,B)$ by simply scaling the synthetic given in Figure 7 to the observed waveforms. Assuming (K = 5), we obtain: $\psi_o(5,1) = 3.1$, $\psi_o(5,2) = 1.7$, and $\psi_o(5,3) = 1.2$ all times 10^{11} cm^3. Next, we will compare the teleseismic waveshapes and amplitudes with these local field results.

TLELSEISMIC RESULTS: t*

The amplitudes of the teleseismic observations, Table 1, show considerable variation. The observed amplitudes vary smoothly with azimuth, Figure 9. The station geometry imposes a strong correlation between azimuth and distance and, hence, a plot of amplitude vs. distance would be a relatively smooth curve where the most distant stations report the largest amplitudes. The observed azimuthal amplitude pattern could be the result of one or all of three mechanisms: 1) strong azimuthal radiation pattern imposed by structure in the source region, 2) effective amplification by the receiver structure for the island stations in the west and northwest azimuths, and 3) lateral variations in t*.

The first mechanism is easily tested by comparing the amplitude behavior of several other events. Figure 9 shows the amplitude data for Jorum, Greeley, Boxcar, Benham and Halfbeak. The absolute amplitude levels for all five data sets have been simultaneously adjusted in order to minimize scatter introduced by varying source strength. These tests were located throughout the Silent Canyon caldera. All five events show a consistent azimuthal trend. Figure 10 shows the waveforms and amplitude ratios for Jorum and Handley. The Handley test was located a few kilometers outside of the boundary faults associated with the caldera. Note that the waveforms are very consistent between these two tests and that the amplitude ratio is stable. We conclude from these

Table 1. Jorum Teleseismic Amplitudes

STA	Dist., Δ (degrees)	AZ (degrees)	Amp. (mμ)	C. Amp. (mμ)
SCP	30.0	71.2	823	823
OGD	32.4	70.0	745	782
COL	33.2	336.1	1074	1142
WES	34.7	67.0	468	511
KIP	39.9	258.7	1097	1298
BEC	42.4	80.7	845	1029
NOR	54.8	10.2	182	255
KTG	56.8	23.7	594	860
AKU	59.9	28.3	365	548
NNA	61.6	134.8	422	645
ARE	68.2	133.1	1268	2131
ESK	71.6	33.6	228	399
AFI	72.8	236.7	548	980
NUR	77.4	18.6	274	507
PTO	77.8	47.3	342	639
TOL	81.3	46.0	685	1352
STU	81.7	32.9	251	491
PEL	82.1	142.6	399	799
SHK	83.9	309.1	868	1779
SEO	85.2	314.5	742	1521
NAT	86.1	99.8	548	1151
GUA	88.6	285.9	868	1870
HNR	90.6	258.7	914	2021

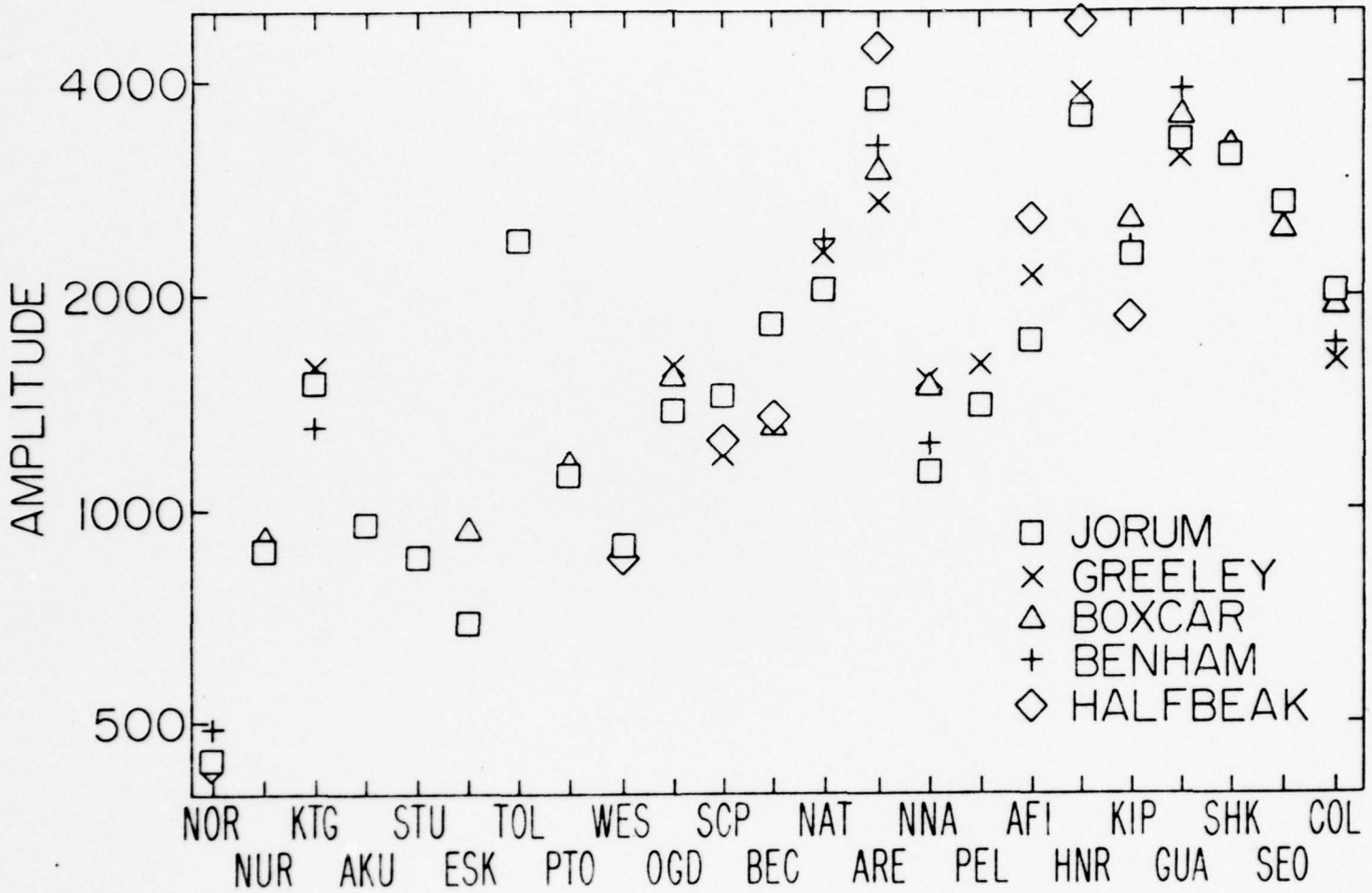

Figure 9: Azimuthal variations in amplitudes as observed for five tests located throughout Pahute Mesa (NOR = 10°, COL = 336°). The absolute amplitudes for each event have been adjusted in order to minimize scatter that results from variations in source strength.

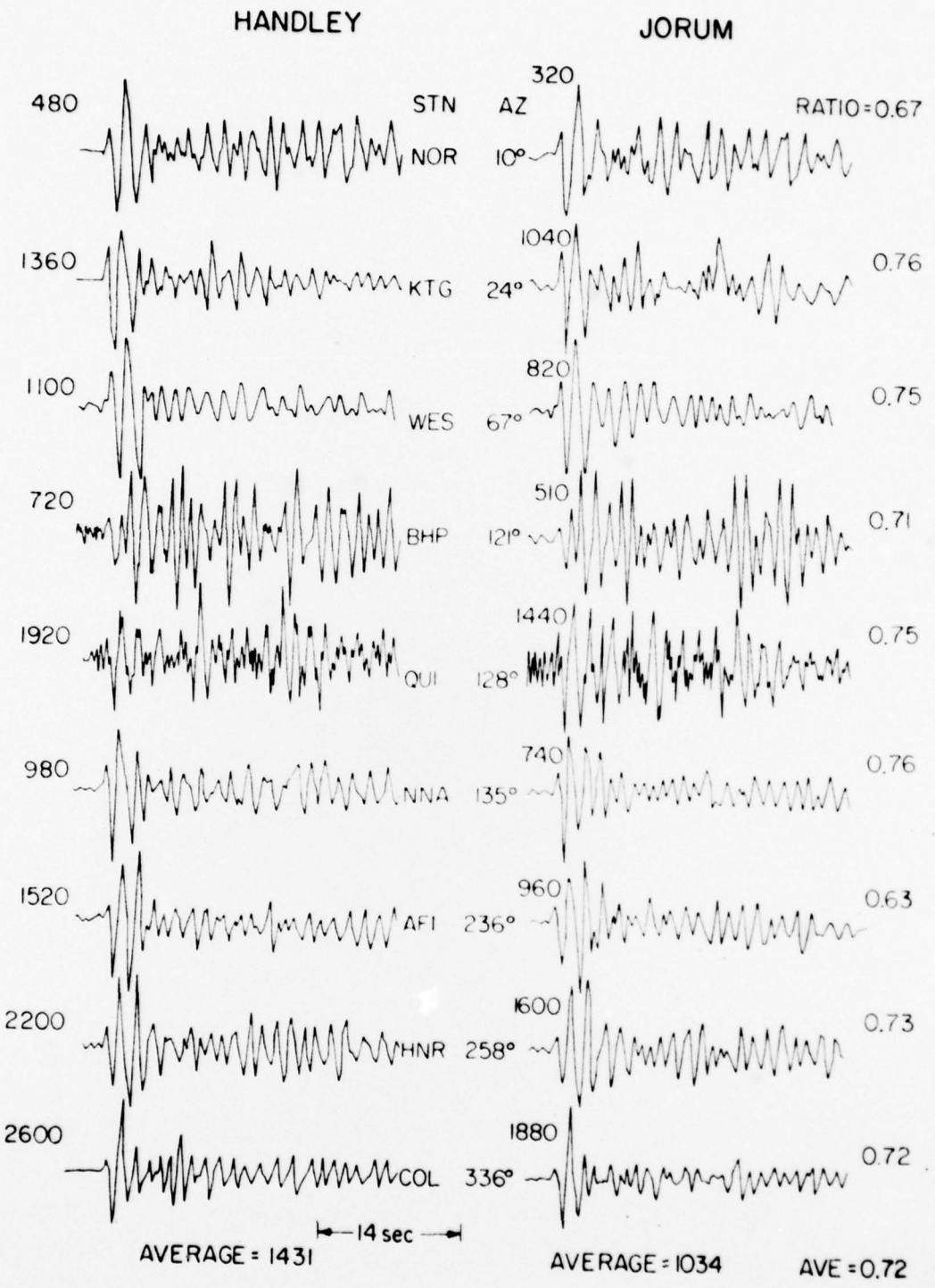

Figure 10: Comparison of the observed teleseismic waveforms and amplitudes for the events Handley and Jorum.

data that source structure is not producing the amplitude anomaly.

The question of systematic bias introduced by receiver structure is difficult to assess on a world wide basis at this stage of study. Short period records can show strong azimuthal patterns as discussed by Helmberger and Wiggins (1971) and Aki (1973) and others. Based on the geology of many of the island stations, significant waveform distortion would not be too surprising. This may in part explain the azimuthal pattern in Figure 9. Fortunately, the stations in the United States have been well studied by Butler (1979) and the east coast stations appear remarkably transparent. Some of the recordings from these stations for the Jorum and Handley events are displayed in Figure 11. The long period observations are quite small on the actual records, whereas the short period observations are nearly off scale. Included at the bottom of Figure 11 are the best-fitting short and long period synthetics we could produce by varying t*. In generating these responses we used the crustal model at the source given in Figure 5 with the velocity below the 4.4 km/sec layer set at 5.1 km/sec. This is also the velocity assumed for the receiver halfspace model. Variations in K and B were not particularly effectual in changing the short period amplitudes because changes in overshoot (B) effect the source strength (ψ_o) determination. That is, increasing the overshoot makes the short period synthetics larger with constant ψ_o, but the source level is effectively

Table 2. Synthetic Teleseismic Amplitudes

K=5	Ampl (mμ)			(SPZ/LPZ)		
	B=1	B=2	B=3	B=1	B=2	B=3
t*						
.8	3145	3162	3153	.81	.84	.84
.9	2520	2507	2529	.73	.76	.76
1.0	2040	2028	2012	.70	.68	.68
1.1	1640	1643	1658	.62	.62	.63
1.2	1351	1350	1362	.56	.56	.57
1.3	1077	1084	1101	.50	.50	.51
1.4	898	902	913	.45	.46	.47
1.5	744	750	768	.41	.42	.43

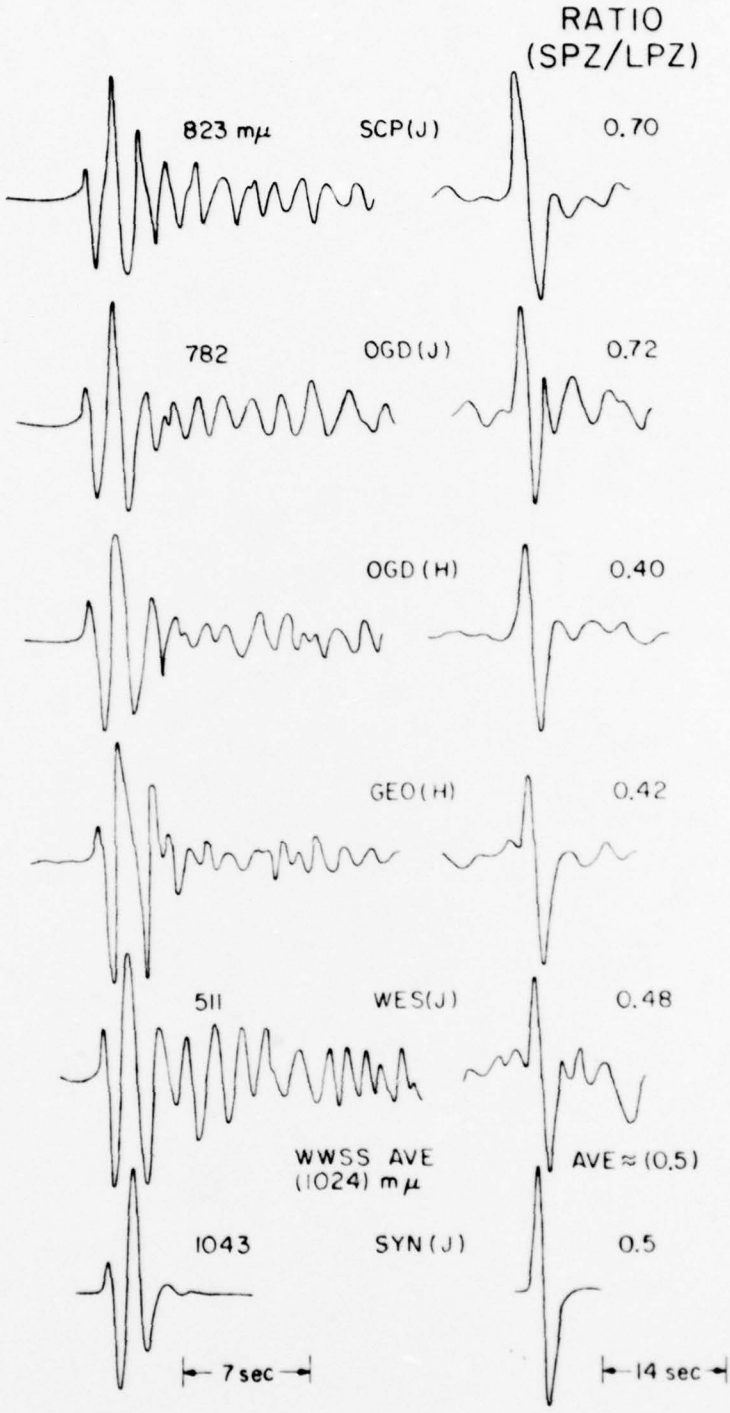

Figure 11: Comparison of the east coast observed waveforms with the synthetic seismograms, assuming $t^* = 1.3$.

smaller because of a compensating scale change required to fit the local amplitudes. Examples of these trade-offs are listed in Table 2 (K = 5, B = 1,2,3). These synthetic teleseismic amplitudes, listed for a range of t* values, can be compared directly with the corrected observed amplitudes in Table 1.

The average corrected amplitude for all short period observations is 1024 mμ. This corresponds to a t* of 1.3, which is significantly larger than previous determination. The systematic azimuthal trend in amplitudes shown in Figure 9 can be interpreted as lateral variations in t*. If the entire anomaly is accounted for in this manner, then t* varies from about 1.5 for northeastern azimuths to 1.1 for northwestern.

The average t* of 1.3 obtained in this study is somewhat larger than that reported by Bache, et. al. (1975). Preliminary results from a similar study of Piledriver, using very near-field velocity time histories, indicates a t* of 1.3. These results are compatible with the Jorum study. The teleseismic source strengths, calculated from the near-field Piledriver data are a factor of two larger than the synthetic far-field pulse generated from the finite difference calculations of S^3 (1975) and used in the previous estimates of t*. Because of this apparent underestimation of the source strength, the attenuation required to bring the calculated amplitudes into agreement with the data was significantly smaller. This discrepancy in source

strength exactly accounts for the t* of 1.05 found by Bache, et. al. (1975).

With the present data set it is impossible to uniquely differentiate real lateral variation in t* from apparent variations introduced by systematic bias in receiver structures. In a recent study by Butler (1979) of amplitudes observed at WWSSN stations in the United States from Soviet nuclear tests, it was found that east coast stations do not show anomalously small amplitudes. However, the stations ALQ and GOL are depressed in amplitude by a factor of 2 to 3. The same study found a similar result from earthquake sources in the Kuriles. These observations suggest as a hypothesis that the upper mantle along the ray paths near the stations ALQ and GOL is typified by low Q. Figure 12 is a gnomic projection showing the Soviet test sites and the U.S. WWSSN stations. Dashed lines from stations ALQ and GOL show the ray paths that are attenuated. Also shown on this figure is the range of azimuths from NTS that have been characterized in this study by low amplitudes and large t* (~1.5). It is very intriguing that the two studies are at least consistent with a low Q region in the upper mantle beneath the central Rocky Mountains. This model is clearly not unique and additional studies of the azimuthal receiver function characteristics of world wide stations will be required to more fully understand the origin of the azimuthal amplitude anomaly observed at the NTS.

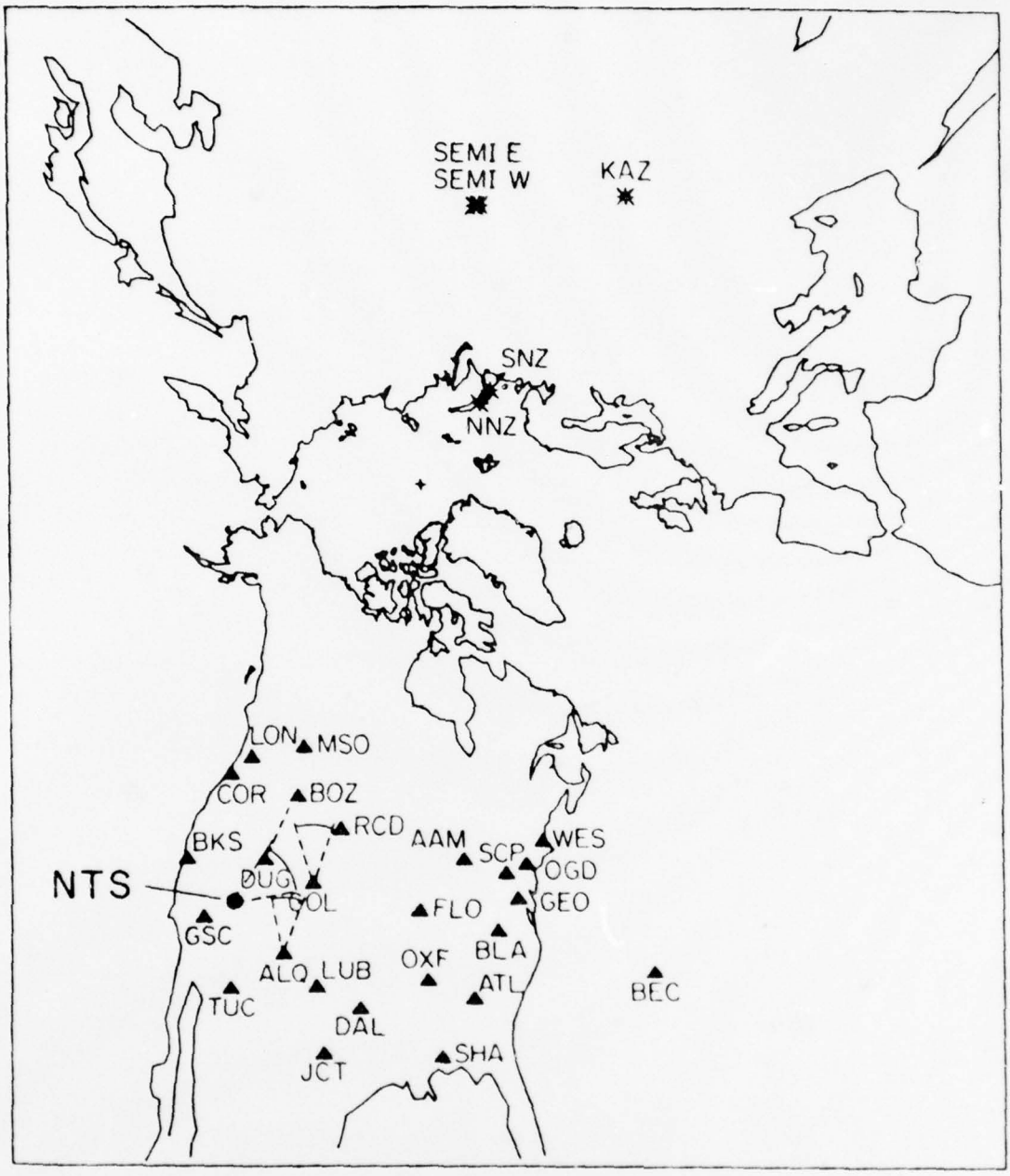

Figure 12: A gnomic projection (all great circles are straight lines) showing the NTS, WWSSN stations of the United States, and the Soviet Union test sites. Butler (1979) has observed a large seismic attenuation at the stations GOL and ALQ, relative to other U.S. stations from sources in both the Soviet Union and the Kuriles (dotted azimuths). World wide stations in a northeast azimuth from NTS are significantly reduced in amplitudes relative to other azimuths.

REFERENCES

Aki, D. (1973), Scattering of P waves under the Montana Lasa, J. Geophys. Res., 8, 1334-1346.

Bache, T. C. and Others. (1974), An explanation of the relative amplitudes of the teleseismic body waves generated by explosions in different test areas at NTS, Systems, Science and Software, Final Report DNA 3958F.

Butler, R. (1979), An amplitude study of Russian nuclear events for WWSSN stations in the United States, Quarterly Technical Report, SGI-R-79001, Sierra Geophysics, Arcadia, CA.

Burdick, L. (1978), t* for S waves with a continental ray path, Bull. Seism. Soc. Am., in press.

Burdick, L. and D. Helmberger (1979), Time functions appropriate for nuclear explosions, Bull. Seism. Soc. Am., in press.

Burdick, L. and G. Mellman (1976), Inversion of the Body waves of the Borrego Mountain earthquake to the source mechanism, Bull. Seism. Soc. Am., 66, 1485-1499.

Carpenter, E., P. Marshall, and A. Douglas (1967), The amplitude-distance curve for short period teleseismic P-waves, Geophys. J. R. astr. Soc., 13, 61-70.

Diment, W., D. Healey, and J. Roller (1960), Gravity and seismic exploration at the Nevada Test Site, U.S. Geol. Survey Prof. Paper 400B, B156-160.

Fraiser, C. and J. Filson (1972), A direct measurement of the earth's short-period attenuation along a teleseismic ray path, J. Geophys. Res., 77, No. 20, 3782-3791.

Haskell, N. (1967), Analytic Approximation for the elastic radiation from a contained underground explosion, J. Geophys. Res., 72, 2583-2597.

Heaton, T. and D. Helmberger (1977), A study of the strong ground motion of the Borrego Mountain California Earthquake, Bull. Seism. Soc. Am., 67, 315-330.

Helmberger, D. and D. Harkrider (1972), Seismic source description of underground explosions and a depth discriminate, Geophys. J. R. astr. Soc., 31, 45-66.

Helmberger D. and R. Wiggins (1971), Upper mantle structure of midwestern United States, J. Geophys. Res., 76, 3229-3245.

Keller, G., (1960), Physical properties of tuffs of the Oak Spring Formation, Nevada, U. S. Geol. Survey Prof. Paper 400B, B396-B400.

Mellman, G. and D. Helmberger, (1974), High-frequence attenuation by a thin high-velocity layer, Bull. Seism. Soc. Am., 64, 1383-1388.

Orkild, P., D. Sargent and R. Snyder (1969), Geologic map of Pahute Mesa, Nevada Test Site and vicinity, Nye County, Nevada, U.S. Geol. Survey, Misc. Geol. invest. map *-567.

Peppin, W. (1974), The cause of the body wave-surface wave discirminant between earthquakes and underground nuclear explosions at near-regional distances, Ph.D. Thesis, University of California at Berkeley.

Peppin, W. (1977), A near-regional explosion source model for tuff, Geophys. J. R. astro. Soc., 48, 331-349.

Spence, W. (1974), P-wave residual differences and inferences on an upper-mantle source for the Silent Canyon Volcanic Centre, Southern Great Basin, Nevada, Geophys. J. R. astr. Soc., 38, 505-523.

Springer, D. and R. Kinnaman (1971), Seismic source Summary for U.S. underground nuclear explosions, 1961-1970, Bull. Seism. Soc. Am., 61, 1073-1098.

Von Seggern, D. and R. Blandford (1972), Source time functions and spectra for underground nuclear explosions. Geophys. J.R. astr. Soc., 31, 83-97.